ISSN 0023-1584, Kinetics and Catalysis, 2006, Vol. 47, No. 4, pp. 511–523. © MAIK "Nauka/Interperiodica" (Russia), 2006.
Original Russian Text © E.Z. Utyanskaya, B.V. Lidskii, M.G. Neigauz, A.E. Shilov, 2006, published in Kinetika i Kataliz, 2006, Vol. 47, No. 4, pp. 528–540.

Simulation of the Kinetics of Adenosine 5'-Triphosphate Hydrolysis Catalyzed by the Cu^{2+} Ion: The Role of Conformation and the Catalytic Effect of the OH^- Ion

E. Z. Utyanskaya[a], B. V. Lidskii[b], M. G. Neigauz[a], and A. E. Shilov[a]

[a] *Emanuel Institute of Biochemical Physics, Russian Academy of Sciences, Moscow, 117977 Russia*
[b] *Semenov Institute of Chemical Physics, Russian Academy of Sciences, Moscow, 117977 Russia*
e-mail: neuhaus@center.chph.ras.ru

Received June 17, 2004

Abstract—The hydrolysis kinetics of the dimeric complex $(CuATP^{2-} \cdot OH_2)_2$ {D} up to ≈40% ATP conversion at 25°C, pH 5.7–7.8, and $[Cu \cdot ATP]_0 = (2.07 \pm 0.03) \times 10^{-3}$ mol/l is analyzed by numerical simulation. $CuADP^- + P_i$ (P_i is an inorganic phosphate) form from DOH^-, and the latter forms rapidly from D. The abstraction of H^+ from the coordinated H_2O molecule is an irreversible reaction involving an OH^- ion from the medium. The maximum possible DOH^- concentration at a given pH is reached at the initial stage of hydrolysis (0.3–6.0 min after the initiation of hydrolysis). $CuADP^- + P_i$ form from D via two consecutive irreversible steps. The ADP buildup rate in the process is determined by the reversible conformational transformation of DOH^- resulting in a pentacovalent intermediate (IntK). OH^- ions from the medium are involved both in IntK formation and in the reverse reaction and are a hydrolysis inhibitor. AMP forms from the intermediate $IntK_3$, which forms reversibly from DOH^-, OH^- ions from the medium being involved in the forward and reverse reactions. This is followed by irreversible $(AMPH)^-$ formation involving H_3O^+ ions from the medium. The rate and equilibrium constants are determined for the formation and decomposition of hydrolysis intermediates. The concentrations of the intermediates are plotted versus time for various pH values. The structures of the intermediates are suggested. The causes of a peak appearing in the initial ADP formation rate versus pH curve are analyzed.

DOI: 10.1134/S0023158406040069

We have already reported a quantitative kinetic study of the hydrolysis of the $(CuATP^{2-} \cdot OH_2)_2$ complex at 25°C [1]. The reaction in that study was conducted up to ≈40% ATP hydrolysis. Two series of experiments were carried out, which differed in the initial Cu · ATP concentration. According to preliminary analysis, the $(CuATP^{2-})_2OH^-$ {DOH^-} complex, which consists of two cyclic monomers $Cy(CuATP^{2-})$, one being deprotonated, is responsible for the formation of $CuADP^- + P_i$ (P_i is an inorganic phosphate) [1]. The highest possible DOH^- concentration at a given pH is reached at the initial stage of hydrolysis. The fraction of this species in the total amount of nucleoside 5'-phosphates as a function of pH passes through a maximum. The formation of ADP from DOH^- proceeds rather rapidly.

Our experimental technique, designations, and the most important data are presented in [1]. Here, we establish the order of hydrolysis steps and, using numerical simulation, determine rate and equilibrium constants for the conversion of hydrolysis intermediates. We present data analysis only for experimental series I at pH 5.7–7.8 [1]. The experimental conditions examined in this work are given in Table 1.

COMPUTATIONAL PROCEDURE

The determination of the rate constants of the reactions examined reduces to solving the inverse problem of chemical kinetics. In our investigation, it was necessary to find a self-consistent reaction network and to fit the reaction rate constants so that the solutions of the direct problems for the rate equations with these constants are sufficiently close to experimental data for ADP and AMP at various pH values. The direct kinetic problem was solved using a standard program realizing our simulation procedure [2]. The problem was solved by directed enumeration of variants, gradually augmenting and complicating the kinetic scheme. Initial variants were limited to the mechanism of the formation of the reactive species DOH^- through the abstraction of H^+ from the coordinated water molecule. We considered kinetic schemes that do or do not take into

Table 1. Experimental conditions for pH 5.7–7.8

Run no.	pH*	$[NuP]_0 \times 10^3$, mol/l	$[Cu^{2+}]_0 \times 10^3$, mol/l	$[NaClO_4]$, mol/l	$[Cu \cdot ATP]_0 \times 10^3$, mol/l	$[CuATP^{2-}]_0 \times 10^3$, mol/l	$w_{0,\,ADP} \times 10^6$, mol l^{-1} min^{-1}	$\tau_{ind,\,AMP}$, min
1	5.70 ± 0.03	2.17	2.11	0.110	2.09	1.97	1.16 ± 0.03	≈140
2	6.00 ± 0.02	2.18	2.11	0.109	2.03	1.93	2.92 ± 0.05	≈46–50
3	6.20 ± 0.04	2.16	2.11	0.108	2.08	1.98	4.24 ± 0.13	≈20
4	6.27 ± 0.03	2.17	2.10	0.109	2.04	1.94	4.31 ± 0.05	≈20
5	6.40 ± 0.02	2.16	2.10	0.105	2.08	1.97	5.43 ± 0.21	≈20
6	6.48 ± 0.02	2.16	2.10	0.108	2.08	1.97	5.17 ± 0.19	≈19
7	6.71 ± 0.01	2.16	2.10	0.105	2.08	1.95	6.33 ± 0.40	≈17
8	6.76 ± 0.03	2.17	2.10	0.117	2.09	1.96	7.90 ± 1.09	≈7
9	6.77 ± 0.03	2.20	2.12	0.119	2.10	1.95	6.53 ± 1.02	≈7
10	6.81 ± 0.03	2.16	2.10	0.111	2.09	1.96	7.23 ± 1.54	6–7
11	6.90 ± 0.02	2.16	2.10	0.112	2.09	1.93	7.29 ± 0.99	≈8
12	7.00 ± 0.03	2.15	2.10	0.110	2.08	1.91	5.85 ± 0.11	≈8
13	7.09 ± 0.03	2.16	2.10	0.105	2.09	1.90	7.06 ± 0.34	≈10
14	7.27 ± 0.04	2.14	2.10	0.107	2.08	1.81	6.48 ± 0.18	7–10
15	7.35 ± 0.02	2.15	2.09	0.109	2.08	1.77	5.86 ± 0.32	7–10
16	7.58 ± 0.03	2.14	2.08	0.108	2.07	1.61	4.66 ± 0.26	≈10
17	7.59 ± 0.02	2.15	2.08	0.109	2.04	1.59	4.56 ± 0.17	≈15
18	7.79 ± 0.02	2.14	2.08	0.106	2.06	1.45	3.53 ± 0.15	15–17

Note: $[NuP]_0$ is the total initial concentration of nucleoside 5'-phosphates; $[NaClO_4]$ is the $NaClO_4$ concentration in the cell; the notation $[Cu \cdot ATP]$ indicates that equivalent amounts of Cu^{2+} and ATP are present in the solution, leaving aside speciation; $[Cu \cdot ATP]_0$ is calculated from the initial ATP mole fraction $\alpha_{0,ATP}$, which is determined derived either by extrapolating the initial linear portion of the ATP consumption curve to $t \longrightarrow 0$ or by analyzing the nucleotide composition of the solution before pH stabilization; $[Cu \cdot ATP^{2-}]_0 = a \times [Cu \cdot ATP]_0$, where a is the mole fraction of $CuATP^{2-}$ in the totality of species at a given pH and 25°C; $w_{0,\,ADP}$ is the initial ADP formation rate derived from the initial linear portion of the ADP buildup curve. The error ranges at the initial rate values are for 95% confidence probability.

* The mean pH value in the run and pH control accuracy.

account the participation of OH^- ions from the medium in the formation of DOH^- and considered only ADP formation curves. Next, we complicated the kinetic scheme by introducing a sequence of AMP formation steps and by taking into account the role of the $[OH^-]$ and $[H_3O]^+$ species of the medium in the formation of intermediates. Both ADP and AMP formation curves were described. The set of rate constants determining the reaction kinetics was determined for each kinetic scheme. An analysis of data obtained for different pH ranges allowed an overall reaction network to be constructed.

RESULTS AND DISCUSSION

Kinetic Scheme Assuming DOH^- Formation through the Spontaneous Detachment of H^+ from the Coordinated H_2O Molecule at the Active Site of the Dimer (Scheme 1)

In calculations for Scheme 1, it was assumed that, in the pH range examined, the dimer D, which consists of

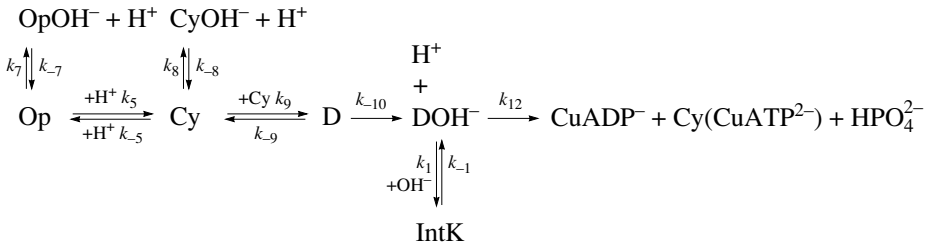

Scheme 1.

two monomeric, cyclic $CuATP^{2-} \cdot OH_2$ molecules, is rapidly equilibrated with open (Op) and cyclic (Cy) monomers. The equilibrium constant of the formation of the complex D from two molecules of the cyclic monomer is $K'_D = [D]_0/[Cy]_0^2 = 200$ l/mol [1]. The formation rate constant of the dimer is as high as $k_9 = 4 \times 10^4$ l mol^{-1} min^{-1}, while $k_{-9} = 200$ min^{-1}. The species Op and Cy are rapidly equilibrated. Their equilibration is catalyzed by the H_3O^+ ion and is characterized by much higher rate constants ($k_5 = 2 \times 10^{10}$ l mol^{-1} min^{-1} and $k_{-5} = 0.98 \times 10^{10}$ l mol^{-1} min^{-1}), like the equilibration of the Op and Cy complexes of $ZnATP^{2-}$ at pH ≤ 8.2 [2–5]. Steps 7 and 8 are the fast protolytic equilibrium reactions involved in the ionization of the coordinated water of the $CuATP^{2-} \cdot OH_2$ monomer. Here, the interaction between ions is diffusion-controlled [6] ($k_{-8} = k_{-7} = 6 \times 10^{10}$ l mol^{-1} min^{-1}). The rate constants of the reverse reactions are calculated from the Op and Cy ionization equilibrium constants [1] to be $k_7 = 602$ min^{-1} and $k_8 = 494.4$ min^{-1}. Scheme 1 includes two slow steps. One is the formation of the reactive species DOH^- via the spontaneous, irreversible abstraction of H^+ from the coordinated water molecule at the active site (rate constant k_{-10}). The decrease in the ADP formation rate during the process is due to the following substitution reaction (second slow step): an OH^- ion adds to Cu^{2+} at the active site, and the N7---Cu^{2+} bond breaks to yield the $Op(OH^-)_2$ complex [4] (here, $D(OH^-)_2$ is designated IntK). The further conversion of IntK was not considered, and only the initial ADP formation rate as a function of pH was analyzed. The rate constants of the formation of ADP from DOH^- and of IntK from DOH^- and OH^- were taken to be $k_{12} = 10$ min^{-1} and $k_1 = 1 \times 10^7$ l mol^{-1} min^{-1}, respectively. It is clear from Fig. 1 that the value of $k_{-10} = 1.8 \times 10^{-2}$ min^{-1} (variant *1*) is in good agreement with the initial rate of ADP formation at the lowest pH value of 6.00 (Fig. 1a). At pH 6.27, the calculated initial rate of ADP formation is below the corresponding experimental value (not shown). At pH 7.00 (Fig. 1b) and 7.35, it is much lower than the experimental value. The value of $k_{-10} = 2.0 \times 10^{-2}$ min^{-1} (variant *4*) is in good agreement with the initial rate observed in run 4 (pH 6.27). For run 2 (pH 6.00), the calculated initial rate of ADP formation is above the experimental value; for pH 7.00 and 7.35, it is well below the experimental value. The value of $k_{-10} = 2.6 \times 10^{-2}$ min^{-1} (variant *2*) provides the best fit to the initial ADP formation rate observed in runs 12 (pH 7.00) and 15 (pH 7.35); however, for runs 4 and 2, the calculated value is much higher than the observed value. Thus, the constant k_{-10}, which describes the initial portion of the ADP formation curve, increases with increasing pH. Therefore, the OH^- ion is involved in the formation of the reactive species DOH^- from D, the deprotonation of the coordinated H_2O molecule at the active site of the dimer does not occur spontaneously, and an OH^- ion from the medium is involved in the abstraction of H^+: $D + OH^- \longrightarrow DOH^- + H_2O$. This reaction is characterized by a bimolecular rate constant k_{-10}. In all schemes considered below, the rate equation for step –10 appears as $k_{-10}[D][OH^-]$.

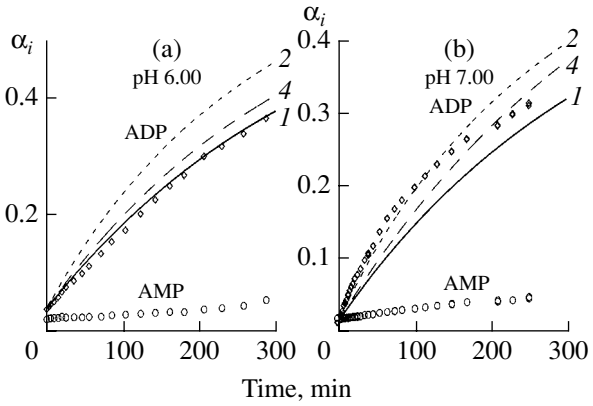

Fig. 1. ADP formation kinetics in runs (a) 2 and (b) 12. The points are experimental data, and the lines represents the data calculated using Scheme 1 for k_{-10} = (*1*) 1.8×10^{-2}, (*2*) 2.6×10^{-2}, and (*4*) 2×10^{-2} min^{-1}. The other rate constants are fixed (see main text).

Kinetic Schemes Taking into Account the Participation of the OH^- Ion of the Medium in the Formation of DOH^-

Unlike calculations for Scheme 1, which were limited to the initial portions of ADP formation curves, calculations for the other schemes covered the entire time interval of product formation. The only difference between Scheme 2 and Scheme 1 is in step –10. Only ADP formation curves are described in Scheme 2 for the reason that, throughout the pH range examined, the initial ADP formation rate is equal to the ATP formation rate within the experimental error (see Table 1 in [1]) and, once an ATP conversion of ≈20–26% is reached in the steady-state hydrolysis regime at pH exceeding pH_{max} in the pH dependence of the initial ADP formation rate, the contribution from AMP formation into the ATP consumption rate doe not exceed 11–14% (see Table 2 in [1]). In this approximation, we used the following rate constants of main reaction steps: $k_{-10} = 1.4 \times 10^6$ l mol^{-1} min^{-1}, $k_1 = 2 \times 10^7$ l mol^{-1} min^{-1}, and $k_{12} = 1$ min^{-1}. The rate constant of step –1 was varied. The assumption that k_{-1} is independent of pH implies that IntK has a structure of the $Op(OH^-)_2$ type, in which the N7---Cu^{2+} bond is broken and the N7 atom is replaced with another OH^- group, as in the case of AMP formation from the monomeric species $Op(OH^-)_2$ resulting from the reversible reaction $CyOH^- + OH^- \Leftrightarrow$

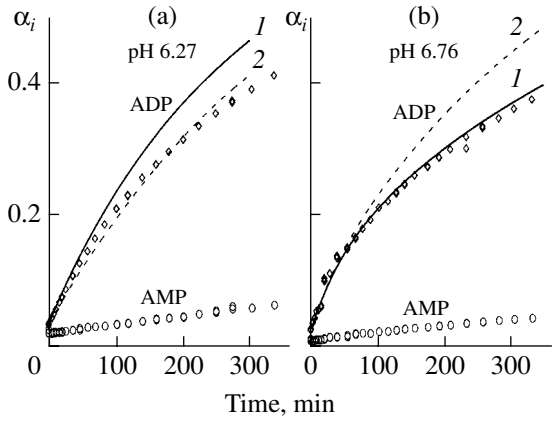

Fig. 2. ADP formation kinetics in runs (a) 4 and (b) 8. The points are experimental data, and the lines represents the data calculated using Scheme 2 for k_{-1} = (*1*) 5×10^{-3} and (*2*) 1×10^{-2} min^{-1}. The other rate constants are fixed (see main text).

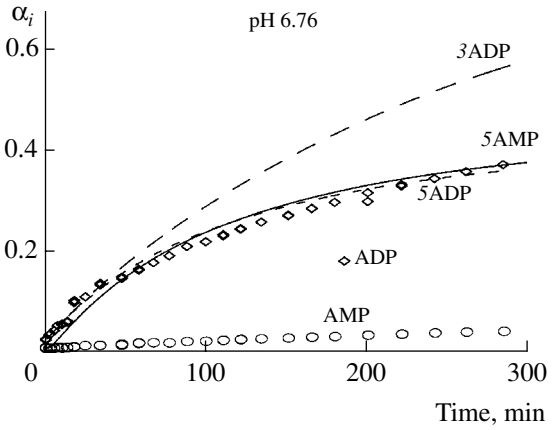

Fig. 3. ADP and AMP formation kinetics in run 8. The points are experimental data. The line *3*ADP represents the data calculated using Scheme 2 (k_{-1} = 0.02 min^{-1}); the lines *5*AMP and *5*ADP represent the data calculated using modified Scheme 2 under the assumption that AMP forms from IntK. k_6 = 0.3 min^{-1} is the rate constant of this reaction in variant *5*, and k_{-1} = 0.02 min^{-1}. The other rate constants are fixed (see main text).

$Op(OH^-)_2$ in the hydrolysis of 5'-ATP catalyzed by Zn^{2+} (see Fig. 4 in [5]). Figure 2 plots experimental ADP formation curves and the curves calculated using Scheme 2 for runs 4 (Fig. 2a) and 8 (Fig. 2b). The best variant for describing run 8 is variant *1* (k_{-1} = 0.01 min^{-1}). In variants *2* (k_{-1} = 0.01 min^{-1}, Fig. 2b) and *3* (k_{-1} = 0.02 min^{-1}, Fig. 3), the k_{-1} values are too large for run 8 and, beyond the initial rate region, the calculated ADP formation curves lie well above the corresponding experimental curves.

Table 2. Parameters of the reactions included in Scheme 5 for calculating the kinetic curves of ADP and AMP formation in the hydrolysis of the dimeric complex $(CuATP^{2-})_2$ consisting of two molecules of the $Cy(CuATP^{2-})$ monomer

No.	Reaction	k_i in Scheme 5	
1	$Op + H^+ \longrightarrow Cy + H^+$	k_5	2×10^{10} l mol^{-1} min^{-1}
2	$Cy + H^+ \longrightarrow Op + H^+$	k_{-5}	0.98×10^{10} l mol^{-1} min^{-1}
3	$Cy + Cy \longrightarrow D$	k_9	4×10^4 l mol^{-1} min^{-1}
4	$D \longrightarrow Cy + Cy$	k_{-9}	200 min^{-1}
5	$D + OH^- \longrightarrow DOH^- + H_2O$	k_{-10}	2×10^6 l mol^{-1} min^{-1}
6	$DOH^- + OH^- \longrightarrow IntK + OH^-$	k_1	2×10^7 l mol^{-1} min^{-1}
7	$DOH^- + OH^- \longrightarrow IntK_3 + OH^-$	k_6	3×10^6 l mol^{-1} min^{-1}
8	$IntK_3 + OH^- \longrightarrow DOH^- + OH^-$	k_{-6}	1×10^4 l mol^{-1} min^{-1}
9	$IntK_3 + H^+ \longrightarrow Cy + (AMPH)^- + Cu^{2+} \cdot (P_2O_7H)^{3-}$	k_3	3×10^4 l mol^{-1} min^{-1}
10	$Op \longrightarrow OpOH^- + H^+$	k_7	602 min^{-1}
11	$OpOH^- + H^+ \longrightarrow Op$	k_{-7}	6×10^{10} l mol^{-1} min^{-1}
12	$Cy \longrightarrow CyOH^- + H^+$	k_8	494.4 min^{-1}
13	$CyOH^- + H^+ \longrightarrow Cy$	k_{-8}	6×10^{10} l mol^{-1} min^{-1}
14	$IntK \longrightarrow IntK_2$	k_2	0.001 min^{-1}
15	$DOH^- \longrightarrow CuADP^- + Cy + HPO_4^{2-}$	k_{12}	0.9 min^{-1}
16	$IntK + OH^- \longrightarrow DOH^- + OH^-$	k_{-1}	1×10^5 l mol^{-1} min^{-1}

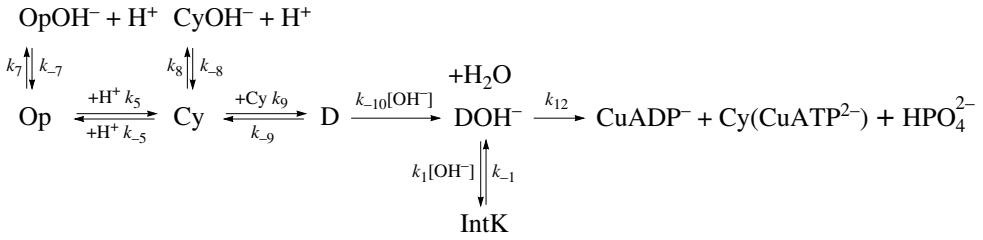

Scheme 2.

A comparison between Fig. 2a and 2b (data calculated using Scheme 2) shows that, other conditions being equal, the ADP formation curve calculated for run 4 (pH 6.27) fits the experimental curve most closely at $k_{-1} = 0.01$ min^{-1} (variant *2*). For run 8 (pH 6.76), the best fit is provided by $k_{-1} = 5 \times 10^{-3}$ min^{-1} (variant *1*). Therefore, the value of the rate constant k_{-1} depends on the concentration of OH^- ions, and the rate equation for step –1 includes $[OH^-]$. Step 1will then appear as

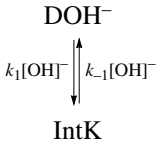

This modification is taken into account in Scheme 3. The further analysis of the kinetic scheme was aimed at finding the optimum values of k_{-1}. Figure 4b demonstrates how the calculated ADP formation curve depends on k_{-1}: in variant *1*, $k_{-1} = 1 \times 10^5$ l mol^{-1} min^{-1}; in variant *2*, $k_{-1} = 1 \times 10^4$ l mol^{-1} min^{-1}; the other rate constants are the same as in Scheme 2 (variants *1* and *2*). Figure 4 (variant *3*) shows how the description of the ADP formation curve in the framework of Scheme 3 can be improved by varying k_{-10} and k_{12} along with k_{-1}. Only ADP formation curves were described in the framework of Scheme 3, while AMP formation curves were left out of consideration.

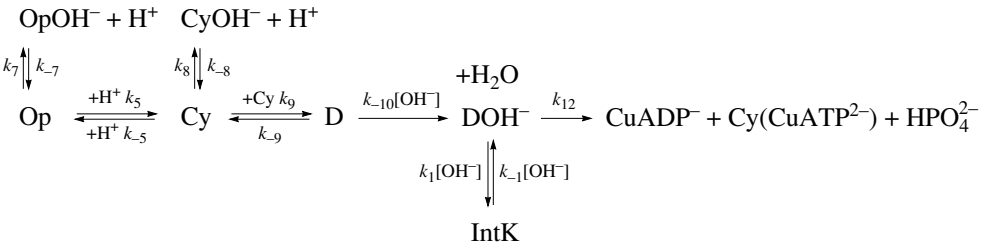

Scheme 3.

Kinetic Schemes Taking into Account the AMP Formation Kinetics

The preliminary analysis of AMP formation curves was carried out within the approximations of Scheme 2, but the step of AMP formation from IntK was added. Figure 3 (variant 5) shows the anomalous run of AMP formation curves calculated under this assumption: after a short induction period, the calculated AMP formation curve lies far above the experimental curve, although the ADP formation curve coincides closely with its experimental counterpart. Therefore, IntK is not an intermediate in AMP formation and the assumption that IntK has a structure of the $Op(OH^-)_2$ type is wrong. It is likely that AMP forms from an intermediate that results from DOH^- rather than IntK.

As compared to Scheme 3 (which adequately describes the ADP formation kinetics), Scheme 4 is complicated to include AMP formation kinetics.

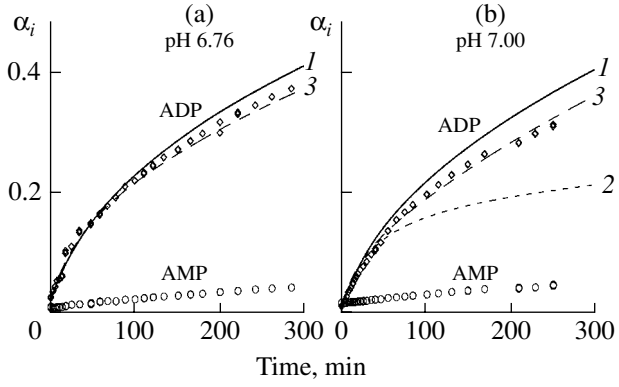

Fig. 4. ADP formation kinetics in runs (a) 8 and (b) 12. The points are experimental data, and the lines represent the data calculated using Scheme 3: (*1*) $k_{-1} = 1 \times 10^5$ l mol^{-1} min^{-1}, $k_{-10} = 1.4 \times 10^6$ l mol^{-1} min^{-1}, and $k_{12} = 1$ min^{-1}; (*2*) $k_{-1} = 1 \times 10^4$ l mol^{-1} min^{-1}, $k_{-10} = 1.4 \times 10^6$ l mol^{-1} min^{-1}, and $k_{12} = 1$ min^{-1}; (*3*) $k_{-1} = 1 \times 10^5$ l mol^{-1} min^{-1}, $k_{-10} = 2 \times 10^6$ l mol^{-1} min^{-1}, and $k_{12} = 0.7$ min^{-1}.

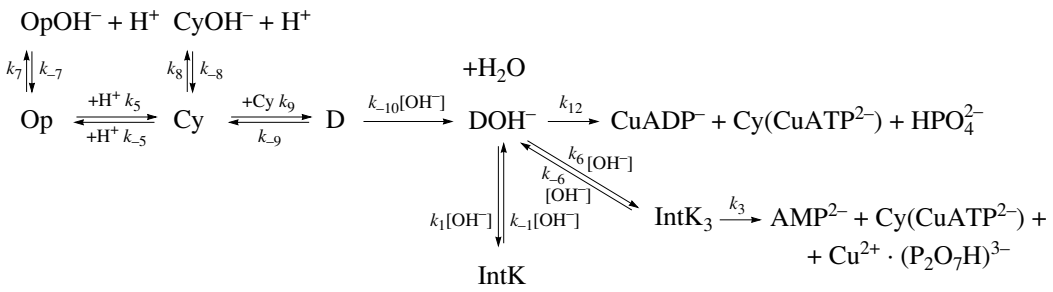

Scheme 4.

It is assumed in Scheme 4 that AMP forms via some intermediate ($IntK_3$) that results directly from DOH^-. The bond between Cu^{2+} and N7 is not broken, and, in $IntK_3$ formation, the OH^- ion located opposite the γ-phosphate group is abstracted and another OH^- ion is attached to Cu^{2+} at the active site opposite the β-phosphate group. This assumption is taken into account in Figs. 5 and 6. The rate equations for the forward step 6 and the reverse step –6 include $[OH^-]$. The equations of steps 6 and –6 are $DOH^- + OH^- \xrightarrow{k_6} IntK_3 + OH^-$ and $IntK_3 + OH^- \xrightarrow{k_{-6}} DOH^- + OH^-$. In step –6, the OH^- ion located opposite the β-phosphate group is abstracted and is replaced by the OH^- ion located opposite the γ-phosphate group. In the intermediate $IntK_3$, the OH^- ion attacks, with the rate constant k_3, the β-P atom to break the $P_\alpha O$---/-P_β bond: $IntK_3 \xrightarrow{k_3} AMP^{2-} + Cy(CuATP^{2-}) + Cu^{2+} \cdot (P_2O_7H)^{3-}$. Step 6, which is the reversible replacement of the OH^- ion opposite the γ-P atom by the OH^- ion located opposite the β-P atom, is, in essence, similar to steps 14 and –14 of the hydrolysis of the $(ZnATP^{2-})_2H^+OH^-$ dimer and $ZnATP^{2-}$ trimer [2, 4, 5]. Figure 5 presents the results of describing the ADP and AMP formation kinetics in terms of Scheme 4. Figures 5a and 5b plot the formation curves calculated for pH 7.58 and 6.27, respectively. The curves were calculated for two variants of rate constants: in variant *1*, $k_6/k_{-6} = 3 \times 10^6 / 5 \times 10^3 = 600$; in variant *2*, $k_6/k_{-6} = 3 \times 10^6 / 1 \times 10^4 = 300$. It is clear from Fig. 5 that, for relatively acidic pH values (in the ascending branch of the initial ADP formation rate versus pH curve), the calculated kinetic curves of ADP and AMP formation are somewhat lower than their experimental counterparts (Fig. 5b). Varying the equilibrium constant of step 6 affects the fit only slightly (see variants *1* and *2* in both plots). At relatively high pH values (in the descending branch of the initial ADP formation rate versus pH curve), the calculated kinetic curves of AMP formation are above their experimental counterparts in both calculation variants (see the run at pH 7.58, Fig. 5a). A similar situation is observed for the two other runs (run 12, pH 7.00; run 3, pH 6.20). Raising k_3 to 0.003 min^{-1} or

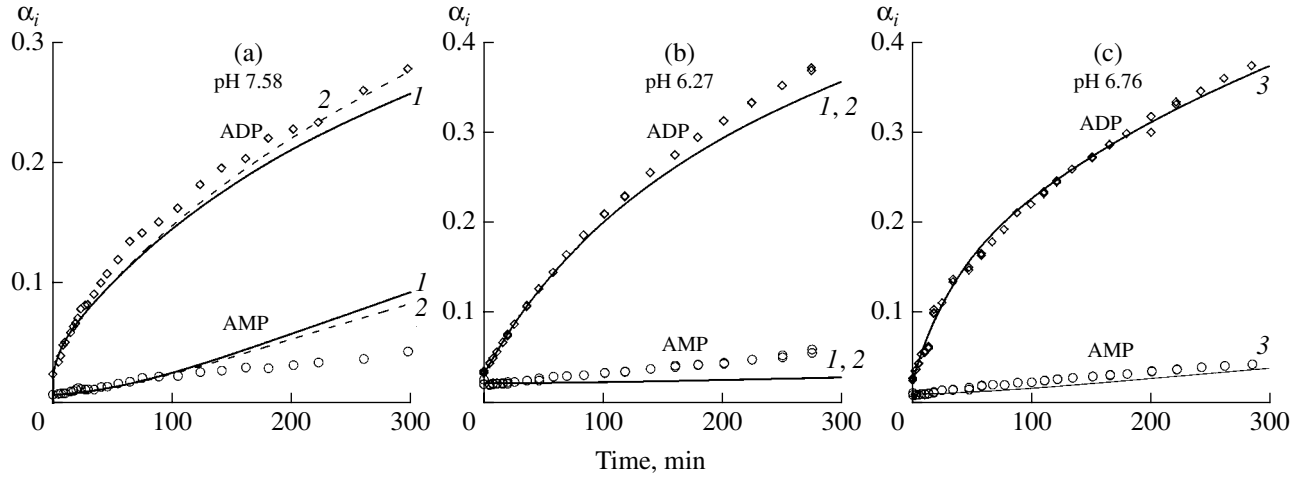

Fig. 5. ADP and AMP formation kinetics in runs (a) 16, (b) 4, and (c) 8. The points are experimental data, and the lines represent the data calculated using Scheme 4: (*1*) $k_{-6} = 5 \times 10^3$ l mol^{-1} min^{-1}, $k_3 = 0.002$ min^{-1}, and $k_{12} = 0.8$ min^{-1}; (*2*) $k_{-6} = 1 \times 10^4$ l mol^{-1} min^{-1}, $k_3 = 0.002$ min^{-1}, and $k_{12} = 0.8$ min^{-1}; (*3*) $k_{-6} = 0.5 \times 10^3$ l mol^{-1} min^{-1}, $k_3 = 0.003$ min^{-1}, and $k_{12} = 0.9$ min^{-1}. The following rate constants are fixed: $k_6 = 3 \times 10^6$ l mol^{-1} min^{-1}, $k_{-10} = 2 \times 10^6$ l mol^{-1} min^{-1}, $k_1 = 2 \times 10^7$ l mol^{-1} min^{-1}, and $k_{-1} = 1 \times 10^5$ l mol^{-1} min^{-1}. The other rate constants are the same as in Scheme 3 (see main text).

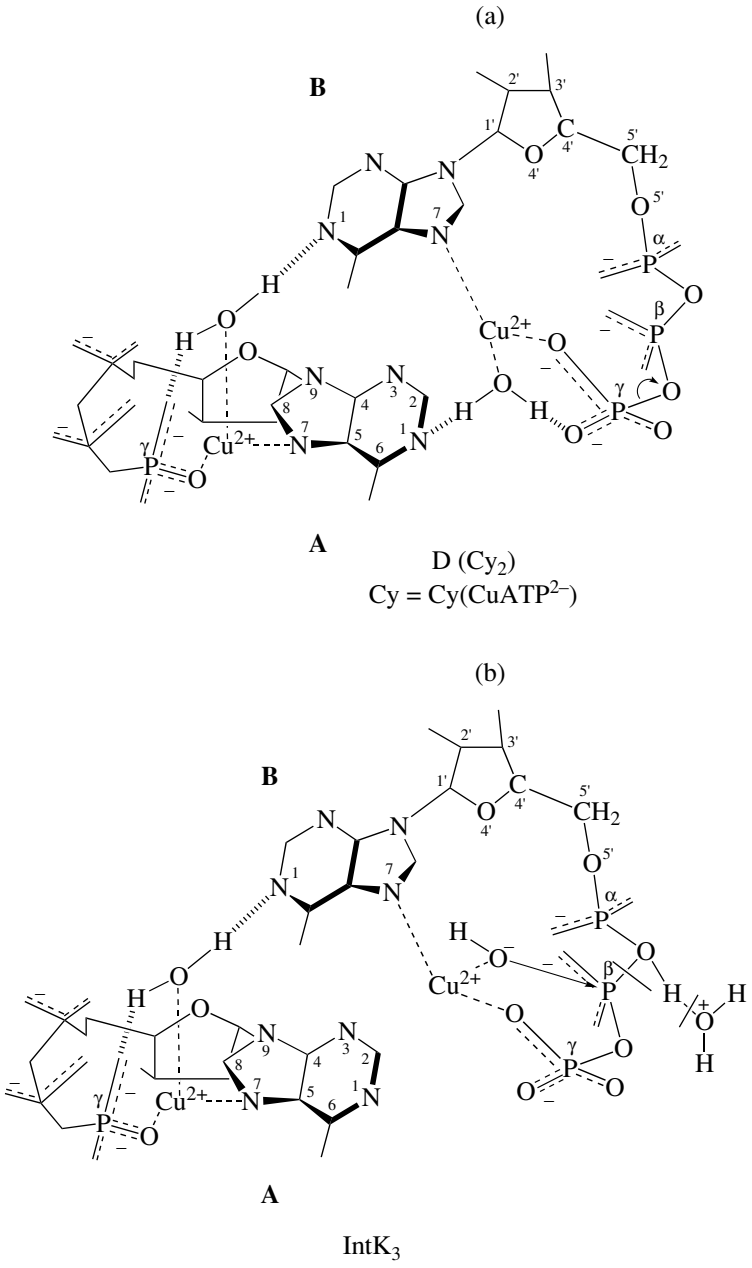

Fig. 6. (a) Assumed structure of the dimer D consisting of two molecules of the Cy(CuATP^{2-}) monomer and (b) structure of the intermediate IntK$_3$ involved in AMP formation.

decreasing k_{-6} to 1×10^3 l mol^{-1} min^{-1} does not change this situation: the calculated AMP formation curve lies below its experimental counterpart for the ascending branch of the initial rate curve and above its experimental counterpart for the descending branch. At pH $\approx$ pH$_{max}$ (pH 6.76, run 8), $k_6 = 3 \times 10^6$ l mol^{-1} min^{-1}, $k_{-6} = 0.5 \times 10^3$ l mol^{-1} min^{-1}, $k_6/k_{-6} = 6000$, $k_3 = 0.003$ min^{-1}, and $k_{12} = 0.9$ min^{-1}, the calculated and observed ADP and AMP formation curves are in satisfactory agreement (Fig. 5c). At the same values of the rate constants, the calculated AMP formation curve is below the experimental curve for pH 6.40 (run 5) and above the experimental curve for pH 7.35 (run 15), as with other values of k_{-6} and k_3 (Figs. 5a, 5b). Extensive calculations have demonstrated that at no k_6 and k_{-6} values can the calculated AMP formation curve be fitted to its experimental counterpart at pH $\approx$ 6 and $\geq$7.0 unless the [H_3O^+] concentration in the medium is included in the rate equation for step 3. Therefore, the selective formation of ADP takes place only in an alkaline medium, when the AMP formation rate is not higher than 15% of w_{ATP}. In a relatively acidic medium, IntK$_3$ forms and is then con-

verted into AMP, involving H^+ ions from the medium. Apparently, the role of H^+ in AMP formation is that it reduces the nucleophilicity of the leaving group by protonating this group during the cleavage of the $P_\alpha O$---/-P_β bond in accordance with the rules of nucleophilic substitution at the P atom [7]. This yields $(AMPH)^-$ + $Cu^{2+} \cdot (P_2O_7H)^{3-}$ + Cy($CuATP^{2-}$) (Fig. 6). The optimum value of the bimolecular rate constant k_3 that provides the best fit to the experimental ADP and AMP formation curves throughout the pH range examined is $k_3 = 3 \times 10^4$ l mol^{-1} min^{-1}, and the AMP formation rate equation appears as $d[AMP]/dt = k_3[H_3O^+][IntK_3]$. The introduction of steps 6, –6, and 3 into the kinetic scheme provides a satisfactory description of the ADP and AMP formation kinetics throughout the pH range examined (Scheme 5).

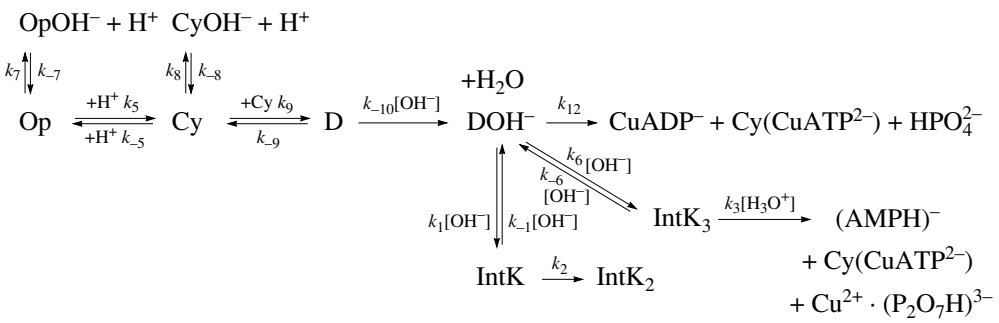

Scheme 5.

The rate constants that are used in calculating the ADP and AMP formation curves for the hydrolysis of the $(CuATP^{2-} \cdot OH_2)_2$ complex in the framework of this final scheme are listed in Table 2. Below, we present the admissible variation ranges for the basic rate constants in Scheme 5: $k_{-10} = (1.7–2.4) \times 10^6$ l mol^{-1} min^{-1}, $k_1 = (1.8–2.2) \times 10^7$ l mol^{-1} min^{-1}, $k_{-1} = (0.8–1.3) \times 10^5$ l mol^{-1} min^{-1}, $k_{12} = 0.8–1.1$ min^{-1}, $k_6 = (2.5–4.0) \times 10^6$ l mol^{-1} min^{-1}, $k_{-6} = (0.2–1.5) \times 10^4$ l mol^{-1} min^{-1}, $k_2 = 0–0.0015$ min^{-1}, $k_3 = (1–5) \times 10^4$ l mol^{-1} min^{-1}, and $k_9 = (3.2–4.8) \times 10^4$ l mol^{-1} min^{-1}.

The likely structures of the reactive hydrolysis intermediates are shown in Figs. 6 and 7. The dimeric complex $(CuATP^{2-} \cdot OH_2)_2$ is assumed to have the same structure as the dimeric complex $D(Cy_2)$ that is formed by two cyclic monomer molecules in the ATP hydrolysis catalyzed by the Zn^{2+} ion (see Fig. 1 in [2]). In the introduction to our earlier publication [2], we presented the likely structures of the cyclic monomeric form of $ZnATP^{2-}$ (Cy), the open monomeric form of $ZnATP^{2-}$ (Op), and the dimeric complex D between two cyclic monomer molecules (the dimer is an intermediate in the pH-independent hydrolysis pathway; see Fig. 1c in [2] and Scheme 2 in [8]). The $D(Cy_2)$ complexes are similar only in the relative positions of the two $MATP^{2-}$ molecules in the dimer, in that the model of the dimer is constructed from two cyclic monomers [2, 8, 9], and in that both are hydrated by the water molecule coordinated to the M^{2+} ion. This M^{2+} ion is bonded to the N7 atom of its own adenine base and to the terminal phosphate group of its own monomer ring. A proton of the H_2O molecule belonging to Cy interacts with the N1 atom of the other ring to establish a hydrogen bond. Similar hydration binds an $MATP^{2-}$ molecule in conformation **A** to the N1 atom of an $MATP^{2-}$ molecule in conformation **B**. At the active site of the dimer, the N1 atom of the adenine base of the second $ZnATP^{2-}$ molecule in conformation **A** abstracts a proton from the coordinated H_2O molecule opposite the γ-phosphate group and transfers it rapidly and reversibly to this γ-phosphate group. This yields a hydrogen bond between the γ-phosphate group bonded to Zn^{2+} and the N1 atom of the second $ZnATP^{2-}$ molecule in conformation **A** ($(ZnATP^{2-})_2H^+OH^-$ complex). Our kinetic data for ATP hydrolysis in the Zn · ATP (1 : 1) system have completely confirmed the dimer model suggested earlier and the role of the N1 atom as the common base catalyst both in the hydrolysis of the dimeric association species and in the hydrolysis of the $ZnATP^{2-} \cdot OH_2$ trimer [2–5, 8, 9]. The kinetic data obtained in this study provide decisive evidence that the reactive nucleophile forms by another mechanism. As distinct from the $(ZnATP^{2-} \cdot OH_2)_2$ dimer, the dimer $(CuATP^{2-} \cdot OH_2)_2$ gives up its proton slowly and irreversibly (step –10). This reaction requires the participation of the OH^- from the aqueous medium, and the P_γ---OP_β bond breaks at the initial stage of hydrolysis at a rate comparable to the formation rate of the reactive nucleophile $Cu^{2+}OH^-$ in the form of DOH^-. As a consequence, $CuADP^-$ forms in two consecutive irreversible steps. The fact that the formation of the reactive species $M^{2+}OH^-$ opposite the P_γ--OP_β bond proceeds at a relatively low rate is evidence that a spatial rearrangement of the coordinated water molecule at the active site of the dimer is necessary. This is also indicated by the cyclic $CuATP^{2-}$ monomer being inactive. As in the case

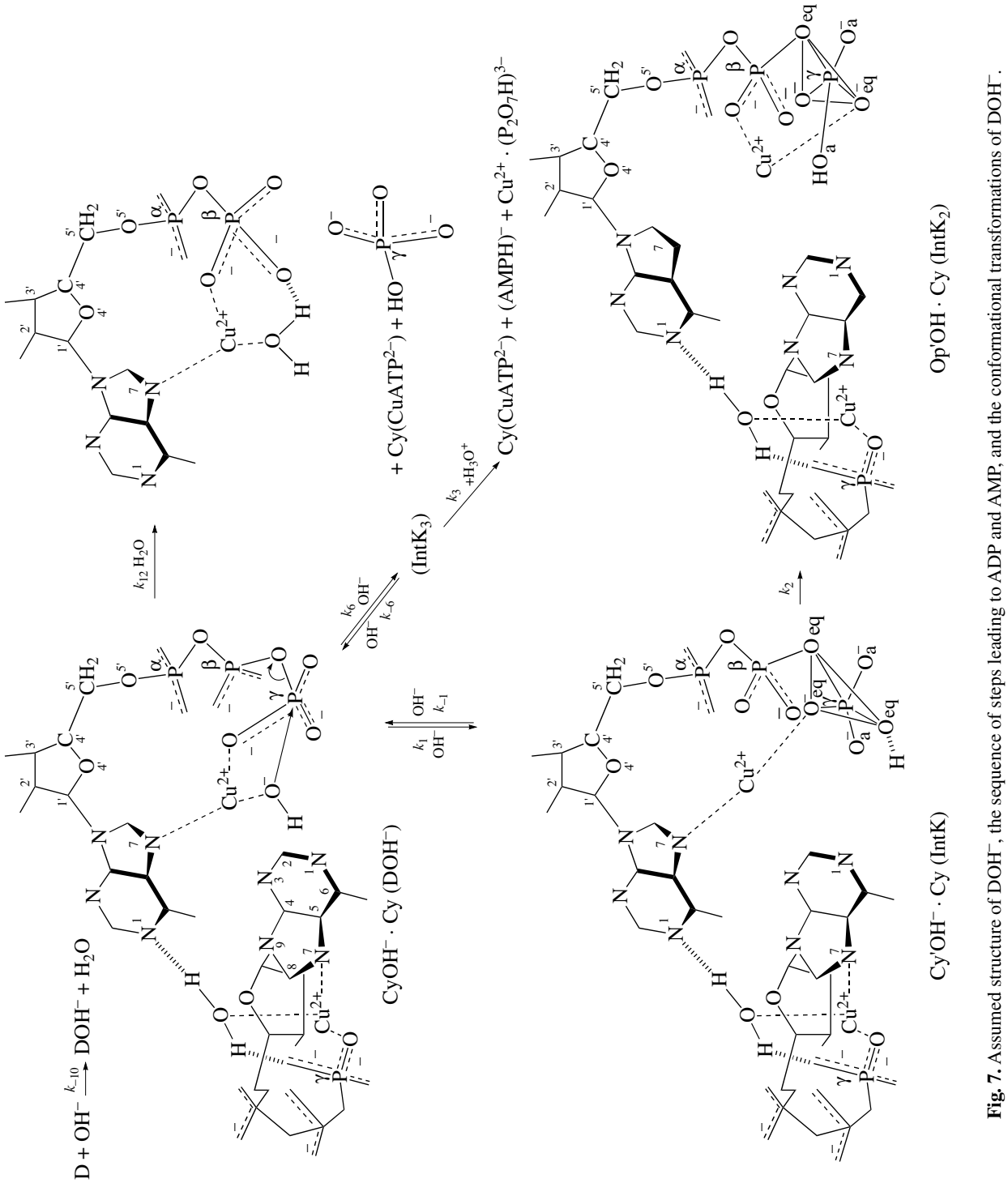

Fig. 7. Assumed structure of DOH^-, the sequence of steps leading to ADP and AMP, and the conformational transformations of DOH^-.

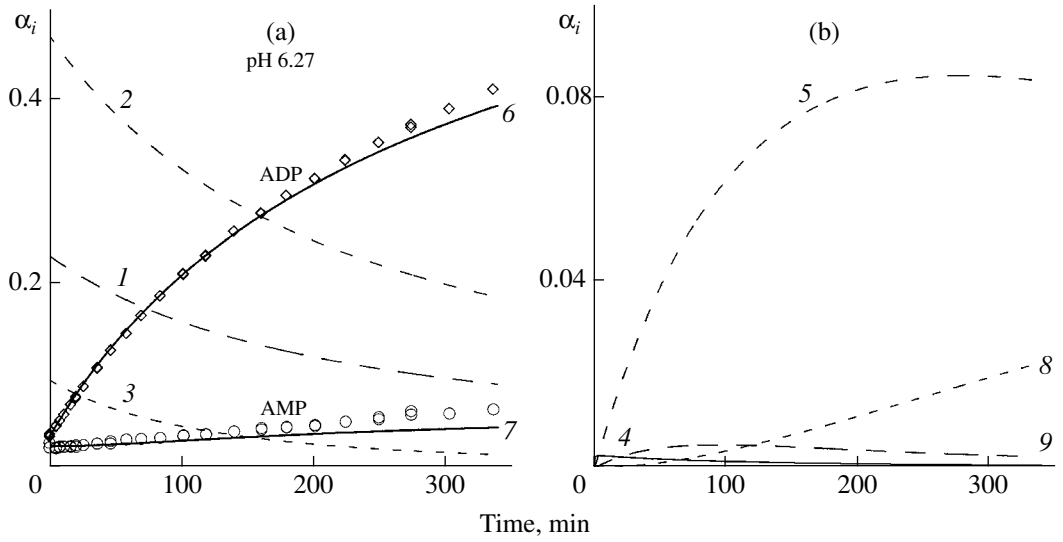

Fig. 8. Variation of the relative amounts of intermediates during hydrolysis at pH 6.27 and 25°C (run 4). $[Cu \cdot ATP]_0 = 2.04 \times 10^{-3}$ mol/l. Intermediates: (*1*) $Op(CuATP^{2-})$, (*2*) $Cy(CuATP^{2-})$, (*3*) D, (*4*) DOH^-, (*5*) IntK, (*6*) ADP, (*7*) AMP, (*8*) $IntK_2$, and (*9*) $IntK_3$. The points are experimental data. The calculation is carried out using Scheme 5. The rate constants are listed in Table 2.

of Zn^{2+}, the coordinated water molecule is located in the hydrophobic moiety of the dimer and is not involved in the hydrogen bonding of water. However, the different mechanisms of reactive nucleophile formation lead to different ratios of the nucleophile formation rate to the rate of nucleophile conversion into ADP. In the Zn^{2+} association species, $CyOH^-$ forms rapidly and irreversibly and the P_γ--OP_β bond cleavage, yielding ADP, occurs at a low rate.

The $CuADP^-$ formation rate constant $-k_{12}$ is pH-independent. Therefore, the attack of $Cu^{2+}OH^-$ on the P_γ--OP_β bond is in-line, yielding a pentacovalent transition state, and must cause a configurational inversion at the γ-P atom of the first molecule. This yields no long-lived pentacovalent intermediates. The relative high value of $k_{12} = 0.9$ min^{-1} is an argument in favor of this interpretation of the elementary step of $CuADP^-$ formation. Pentacovalent intermediates result from the conformational transformations of the reactive dimeric complex $(CuATP^{2-})_2OH^-$. Note that step 1 (Fig. 7) is catalyzed by the OH^- ion of the aqueous medium and is essentially reversible, and the equilibrium in this step is shifted to the IntK complex. In this IntK complex, the bond between Cu^{2+} and the N7 atom of its adenine base is intact. An OH^- ion from the medium adds to its γ-phosphate group, displacing the OH^- group bonded with Cu^{2+} at the active site into the medium. The OH^- ion adds in such a way that the resulting O^-–P_γ bond is in the apical position relative to the terminal phosphate (P_γ). The resulting pentacovalent intermediate (IntK) is structurally similar to the $Cy'OH^-$ species, which forms at pH ≥ 8.5 in ATP hydrolysis catalyzed by the Zn^{2+} ion (Scheme 1a in [2]). The composition of the dimeric complex IntK is $Cy'OH^- \cdot Cy(CuATP^{2-})$. However, since the H^+ affinity is higher at the equatorial site of IntK, the H^+ atom of OH^- is bonded to the O^- ion at the equatorial site of IntK. The $Cy'OH^-$ fragment of IntK is structurally similar to the $Cy'OH^-$ monomer resulting from ATP hydrolysis in an alkaline medium (pH ≥ 8.5) catalyzed by the Zn^{2+} ion. The $Cy'OH^-$ ion, as judged from the behavior of its monomeric form, is readily pseudorotated to form $Op'OH^-$. This species readily substitutes the OH^- group bonded to Zn^{2+} for the OH^- group at the P_γ atom, yielding $OpOH^-$ (Scheme 1a in [2]). ATP hydrolysis catalyzed by the Cu^{2+} ion takes place in a much more acidic pH range than ATP hydrolysis catalyzed by the Zn ion. However, the above pseudorotation is not ruled out for IntK. We assume that such pseudorotation yields $\{Op'OH^- \cdot Cy(CuATP^{-2})\}$ ($IntK_2$) and designates the rate constant of this reaction k_2. In Scheme 5, this reaction is taken into account by introducing reaction 14 (Table 2). However, it turned out that the pseudorotation rate constant k_2 of IntK is as small as 0.001 min^{-1} and offers a very small correction to the ADP formation kinetic curve only at pH ≥ 7.35.

The rate constant of the conformational transformation of the active complex is strikingly high ($k_1 = 2 \times 10^7$ l mol^{-1} min^{-1}), and the equilibrium in step 1 is noticeably shifted to IntK. The final kinetic description (Scheme 5) shows that the OH^- ion of the medium is a powerful inhibitor of $CuADP^-$ formation. Thus, the formation of considerable amounts of the pentacovalent intermediate only slows down the formation of $CuADP^-$.

The selective formation of $CuADP^-$ takes place only in a comparatively alkaline medium (above the pH_{max}

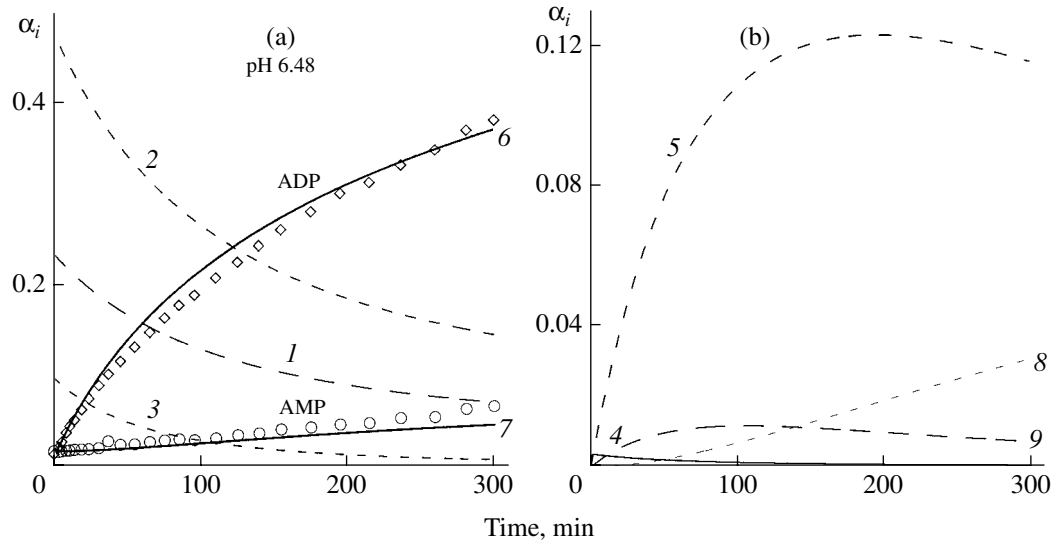

Fig. 9. ADP and AMP formation kinetics and the variation of the concentrations of intermediates in run 6. The intermediates are designated in the same way as in Fig. 8. The points are experimental data.

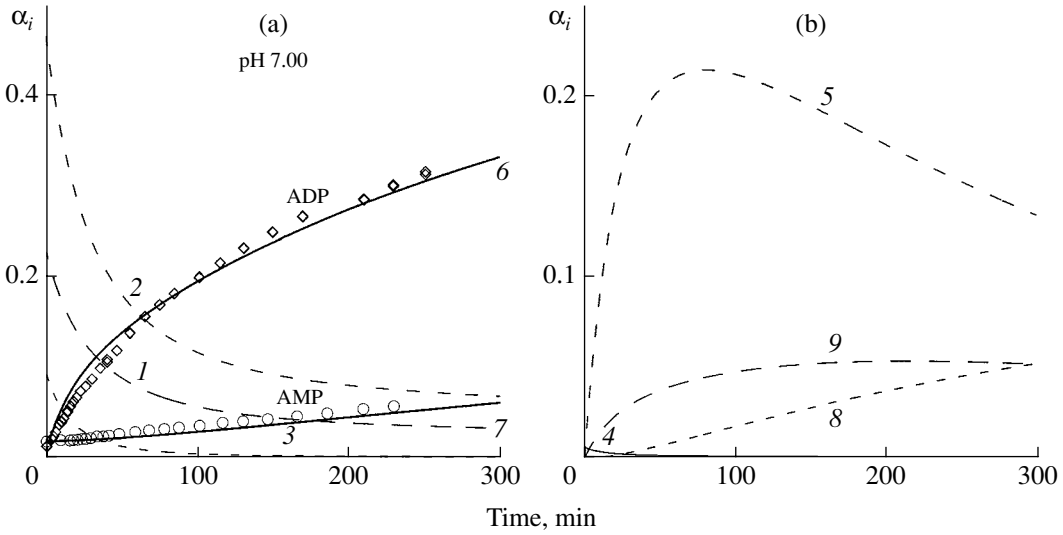

Fig. 10. ADP and AMP formation kinetics and the variation of the concentrations of intermediates in run 12. The intermediates are designated in the same way as in Fig. 8. The points are experimental data.

point in the initial $CuADP^-$ formation rate versus pH curve), the percentage of AMP being low. More acidic media are unfavorable for selective $CuADP^-$ formation. The formation of IntK is also catalyzed by the OH^- ion; however, since step 3 of $IntK_3$ conversion involves H^+ ions from the medium, $(AMPH)^-$ forms mainly in relatively acidic media.

As judged from the small value of k_2, IntK pseudorotation plays a negligible role in the conformational transformations of the reactive intermediates of hydrolysis under the given conditions. At present, we do not know the factors favoring pseudorotation and the further decomposition of the active species IntK. The reversible reaction 1 is a way of saving ATP. It can be assumed that processes of this type, which are inherently reversible, slow down and terminate the hydrolysis of the active species $MATP^{2-}OH^-$ and then cause the desorption of the active complex $MATP^{2-}OH^-$ or the passage of the resulting ATP into the aqueous medium.

Figures 8 and 9 show how the calculated concentrations of the main intermediates and final products (ADP and AMP) vary during hydrolysis at relatively low pH values (6.27 and 6.48). The mole fractions of species in all figures are fractions of the initial nucleoside 5'-phosphate concentration. For comparison, we present the experimental kinetic curves of ADP and AMP forma-

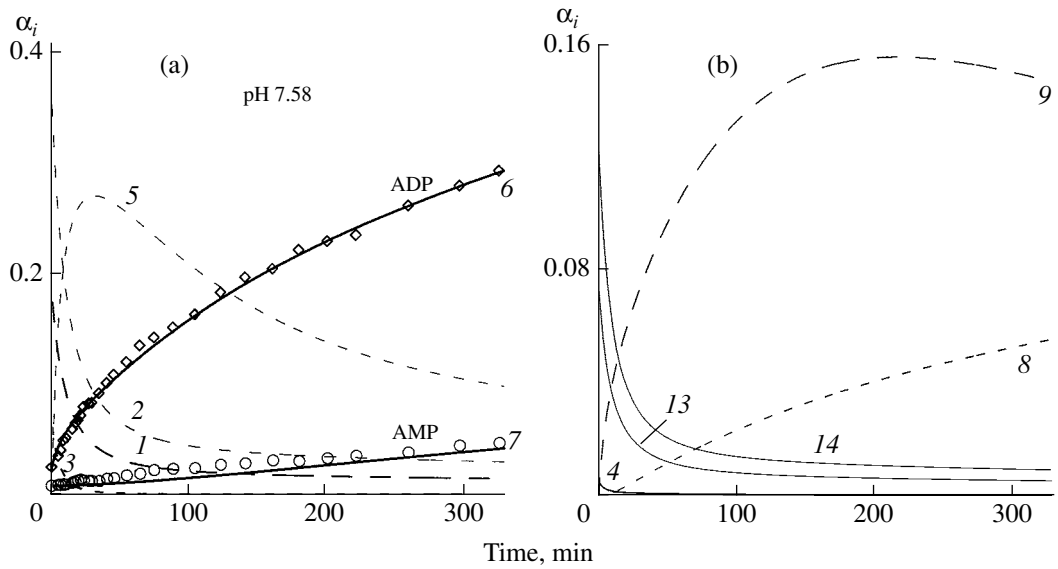

Fig. 11. ADP and AMP formation kinetics and the variation of the concentrations of intermediates in run 16. The intermediates are designated in the same way as in Fig. 8 plus (*13*) $OpOH^-$ and (*14*) $CyOH^-$. The points are experimental data.

tion. The initial ADP formation rate reflects the DOH^- formation kinetics in step –10 and the DOH^- consumption kinetics in step 12. Reactions –10 and 12 in the sequence of ADP formation steps are irreversible. In the pH range examined (in the ascending branch of the $w_{0,\,ADP}$ curve), the DOH^- formation rate exceeds the rate of DOH^- conversion into ADP and IntK only at very early stages of hydrolysis (until the maximum DOH^- concentration is reached in 2.1 min at pH 6.48 (Fig. 9)), $w_{form.ADP} = 7.0 \times 10^{-6}$ mol l^{-1} min^{-1}, $w_{form.DOH^-} = 12.6 \times 10^{-6}$ mol l^{-1} min^{-1}, and $w_{form.IntK} = 4.75 \times 10^{-6}$ mol l^{-1} min^{-1}. After 2.1 min, DOH^- is spent both in the formation of the pentacovalent intermediate IntK and in the formation of ADP, the IntK and ADP formation rate being comparable.

Table 3. Maximum DOH^- mole fraction ($[DOH^-]_{max}/[NuP]_0$) and DOH^- peaking time as a function of PH as calculated using Scheme 5

Run no.	pH	DOH^- peaking time, min	$[DOH^-]_{max}/[NuP]_0$
1	5.70	6.0	3.65×10^{-4}
2	6.00	4.0	1.86×10^{-3}
4	6.27	3.1	2.63×10^{-3}
6	6.48	2.1	3.62×10^{-3}
7	6.71	1.05	4.76×10^{-3}
8	6.76	1.00	5.09×10^{-3}
10	6.81	1.06	5.39×10^{-3}
11	6.90	1.06	5.66×10^{-3}
12	7.00	1.06	5.94×10^{-3}
13	7.09	1.06	6.76×10^{-3}
14	7.27	1.06	6.27×10^{-3}
15	7.35	0.54	6.10×10^{-3}
16	7.58	0.31	5.39×10^{-3}
18	7.79	0.28	4.76×10^{-3}

The AMP buildup rate reflects the $IntK_3$ consumption kinetics after the induction period in $IntK_3$ accumulation. The decrease in the ADP buildup rate is due to an increase in the IntK concentration (Figs. 8, 9). Figure 10 shows the concentration profiles of hydrolysis intermediates near the peak of the initial ADP formation rate versus pH curve (pH 7.00). Figure 11 plots the same profiles for the descending branch of the $w_{0,\,ADP}$ curve (pH 7.58).

The DOH^- concentration peaks very close to the zero time point. It increases with increasing pH in the ascending branch of the $w_{0,\,ADP}$ curve, peaks at pH 7.09 (above the pH value corresponding to the maximum initial ADP formation rate, pH 6.76), and then decreases with increasing pH (Table 3). Some contribution to the DOH^- consumption rate is made by $IntK_3$ formation. The main contribution to the DOH^- consumption rate in the initial portion of the ADP buildup curve in the comparatively acidic region (pH 5.70–6.48) is from IntK formation. The relative contribution from $IntK_3$ is significant starting at pH 6.76–7.00. At pH ≥ 7.35, the contributions from IntK and $IntK_3$ at the initial hydrolysis stage are comparable. These contributions are responsible for the marked decrease in the ADP formation rate at pH ≥ 6.76. Therefore, the peak of the initial ADP formation rate at pH 6.76 is due to reactions 1 and 6 in Scheme 5, whose rate equations include the concentration of OH^- ions. As hydrolysis proceeds, the mole

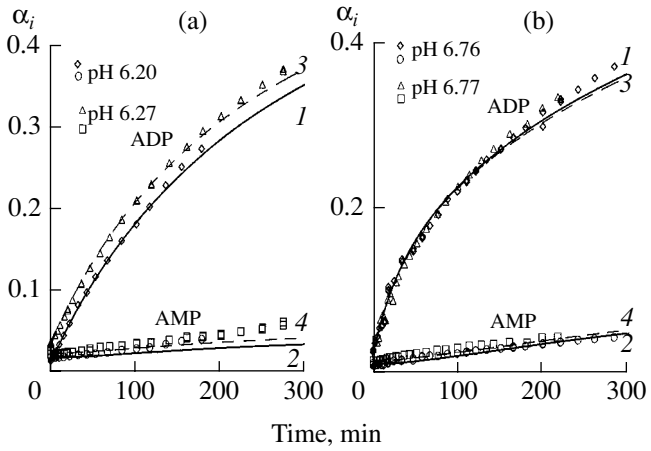

Fig. 12. Experimental (points) and calculated (lines) kinetic curves for ADP and AMP formation: (a) runs 3 ((*1*, *2*) calculated data) and 4 ((*3*, *4*) calculated data); (b) runs 8 ((*1*, *2*) calculated data) and 9 ((*3*, *4*) calculated data). The calculation is carried out using Scheme 5.

fractions of IntK and $IntK_3$ formed from DOH^- pass through a maximum (Figs. 8–11). As pH increases, the IntK peaking time shortens and the peak value of the IntK mole fraction increases. This is accompanied by an increase in the $IntK_3$ mole fraction. At pH >7.09, the mole fractions of IntK and $IntK_3$ are comparable (Fig. 11).

Figure 12a illustrates the coincidence between experimental ADP and AMP formation curves (shown as symbols) and their calculated counterparts (line) in two runs (nos. 3 and 4) conducted at very similar pH values in a relatively acidic pH region. In Fig. 12b, we demonstrate the almost complete coincidence between the experimental and calculated kinetic curves in two runs conducted at nearly the same pH (pH 6.76 in run 8 and pH 6.77 in run 9).

The most significant results of this study are the following:

(1) In the hydrolysis of the dimeric complex $(CuATP^{2-} \cdot OH_2)_2$ in an aqueous medium, $CuADP^-$ forms in two consecutive irreversible steps. The formation of the reactive species DOH^- involves an OH^- ion from the medium.

(2) The kinetic data presented here suggest the irreversible formation of the pentacovalent intermediate IntK from DOH^- during hydrolysis. IntK formation from DOH^- and the reverse reaction (IntK conversion into DOH^-) involve OH^- ions from the medium.

REFERENCES

1. Utyanskaya, E.Z., Lidskii, B.V., Goryachev, S.V., et al., *Kinet. Katal.*, 2006, vol. 47, no. 4 [*Kinet. Catal.* (Engl. Transl.), vol. 47, no. 4].
2. Utyanskaya, E.Z., Lidskii, B.V., Neigauz, M.G., et al., *Kinet. Katal.*, 2000, vol. 41, no. 4, p. 511 [*Kinet. Catal.* (Engl. Transl.), vol. 41, no. 4, p. 462].
3. Utyanskaya, E.Z., Lidskii, B.V., and Neigauz, M.G., *Kinet. Katal.*, 2002, vol. 43, no. 3, p. 346 [*Kinet. Catal.* (Engl. Transl.), vol. 43, no. 3, p. 316].
4. Utyanskaya, E.Z., Shilov, A.E., Lidskii, B.V., et al., *ACH—Models Chem.*, 1996, vol. 133, no. 4, p. 365.
5. Utyanskaya, E.Z., Lidskii, B.V., Neihaus, M.G., et al., *J. Inorg. Biochem.*, 2000, vol. 81, no. 1, p. 239.
6. Bell, R.P., *The Proton in Chemistry*, London: Chapman and Hall, 1973, p. 355.
7. Westheimer, F.H., in *Rearrangements in Ground and Excited States*, Mayo, R., Ed., New York: Academic, 1980.
8. Utyanskaya, E.Z., Pavlovskii, A.G., Sosfenov, N.I., et al., *Kinet. Katal.,* 1989, vol. 30, no. 6, p. 1343.
9. Utyanskaya, E.Z., Mikhailova, T.V., Pavlov, A.O., et al., *ACH—Models Chem.*, 1996, vol. 133, nos. 1–2, p. 65.